Journal of Alloys and Compounds 515 (2012) 74–79

Contents lists available at SciVerse ScienceDirect

Journal of Alloys and Compounds

journal homepage: www.elsevier.com/locate/jallcom

Optical spectroscopy of Tm^{3+} in a locally disordered $Li_2Gd_4(MoO_4)_7$ crystal: A candidate for tunable and ultrafast pulse lasers

Wang Zhao[a], Weiwei Zhou[a], Xinyang Huang[b], Guofu Wang[c,*], Yi Yu[c], Lingyun Li[c], Jianhua Huang[c], Jianming Du[a], Haijun Yu[a], Zhaocheng Lv[a], Yonghong Chen[a]

[a] Anhui Key Laboratory of Low Temperature Co-fired Materials, Departments of Physics, Chemistry & Chemical Engineering, Huainan Normal University, Huainan, Anhui 232038, PR China
[b] Institute of Research on the Functional Materials, Jiangxi University of Finance and Economy, Nanchang, Jiangxi 330013, PR China
[c] Key Laboratory of Optoelectronic Materials Chemistry and Physics, Fujian Institute of Research on the Structure of Matter, Chinese Academy of Sciences, Fuzhou, Fujian 350002, PR China

ARTICLE INFO

Article history:
Received 23 July 2011
Received in revised form
12 November 2011
Accepted 14 November 2011
Available online 22 November 2011

PACS:
42.62.Fi
42.70.Hj
81.10.Fq

Keywords:
Optical spectroscopy
Czochralski method
Molybdates
Solid-state laser materials

ABSTRACT

The optical properties of a locally disordered Tm^{3+}:$Li_2Gd_4(MoO_4)_7$ crystal have been investigated extensively to assess its feasibility of efficient ultrafast laser operation in the 2 μm spectral region. The main spectroscopic parameters relevant to laser applications have been evaluated by analyzing the polarized absorption spectra using the Judd–Ofelt theory. The cross-relaxation mechanisms between Tm^{3+} levels have been applied to analyze the lifetimes of the $^3F_4$, $^3H_4$, and $^1G_4$ manifolds. The potential for producing subpicosecond laser pulses has been discussed on the basis of the calculated emission and gain cross-sections around 2 μm wavelength. The crystal exhibits broad optical bandwidths, large absorption/emission cross sections, and a long $^3F_4$ fluorescence lifetime. All these features indicate that the Tm^{3+}:$Li_2Gd_4(MoO_4)_7$ crystal is a promising gain medium for tunable and ultrafast (fs) pulse lasers.

1. Introduction

With the rapid development of solid-state laser technologies, numerous materials have been extensively exploited for potential laser applications in various wavelength regions from the ultraviolet to the infrared [1–7]. Ultrafast laser sources operating in the eye-safe 2 μm spectral range have aroused considerable attention due to their important applications in metrology, medical diagnostics, soft X-ray generation, time-resolved molecular spectroscopy, etc. [8]. Among optically active ions emitting around 2 μm, Tm^{3+} has demonstrated to be a very attractive candidate. Major advantages with Tm^{3+}-doped matrices include the availability of a AlGaAs laser diode (LD) pumping via the $^3H_6 \rightarrow {}^3H_4$ transition, the pump quantum efficiency approaching 2 associated with a favorable cross-relaxation (CR) process ($^3H_4 + {}^3H_6 \rightarrow {}^3F_4 + {}^3F_4$), a long lifetime of the $^3F_4$ upper laser level, and a wide tunability near 2 μm [9]. All these features make Tm^{3+} advantageous for developing LD-pumped tunable and ultrafast pulse lasers. Indeed, pulse duration as short as 173 fs has been achieved in a stretched-pulse Tm^{3+}-doped fiber laser [10]. However, the typical pulse duration generally obtained from the Tm^{3+}-doped crystals is picosecond level, for instance, 10-ps and 35-ps pulses have been realized for the Tm^{3+}:$KLu(WO_4)_2$ crystal [11] and the Tm^{3+}:YAG crystal [12], respectively. It is widely known that the ultrafast pulse duration depends critically on the optical bandwidths of gain media. Materials with local disorder exert a spatially variable crystal field on the lasant ion, resulting in additional inhomogeneously broadened spectral bands [13–15]. Therefore, current interest is devoted to Tm^{3+}-doped disordered crystals for further reducing the achievable laser pulse duration [14,15].

The tetragonal scheelite-type double molybdate (DMo) and double tungstate (DT) crystals with the general formula $M^+T^{3+}(X^{6+}O_4)_2$ (X = Mo or W), are attractive laser host materials with structural disorder arising from the random distribution of M^+ and T^{3+} cations [14,16–19]. These crystals hold great promise for efficient tunable and femtosecond mode-locked Yb^{3+} laser

* Corresponding author. Tel.: +86 591 83714636; fax: +86 591 83714636.
E-mail address: wgf@ms.fjirsm.ac.cn (G. Wang).

0925-8388/$ – see front matter © 2011 Elsevier B.V. All rights reserved.
doi:10.1016/j.jallcom.2011.11.065

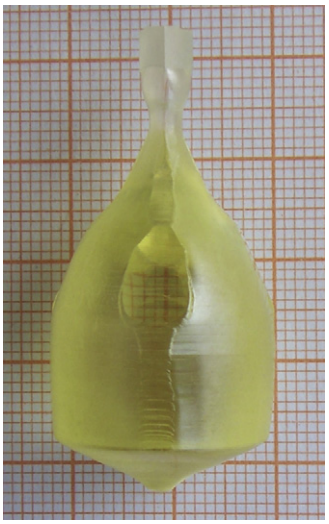

Fig. 1. As-grown Tm^{3+}:$Li_2Gd_4(MoO_4)_7$ crystal.

operation under Ti-sapphire and LD pumping. As an example, a pulse duration of 91 fs at 1026 nm and a tuning range from 1005 to 1059 nm have been presented for the Yb^{3+}:$NaY(MoO_4)_2$ crystal [19]. $Li_2Gd_4(MoO_4)_7$, also expressed as $Li_{0.286}Gd_{0.571}Ø_{0.143}MO_4$ (Ø stands for the vacancies in the cation sites), is a scheelite-type solid solution with space group $I4_1/a$ and cell parameters: $a = b = 5.2081$ Å, $c = 11.4210$ Å [20,21]. Unlike the aforementioned DMo and DT crystals, a cation site in the title crystal is occupied by 0.286Li, 0.571Gd, and 0.143Ø [21], thus leading to a high degree of structural disorder. This inevitably contributes to inhomogeneous broadening of the absorption and fluorescence spectra, which brings a large number of advantages from the standpoint of application as an active medium in LD-pumped mode-locked solid-state lasers. The purpose of the present work is to provide and discuss the spectroscopic features of the Tm^{3+}:$Li_2Gd_4(MoO_4)_7$ crystal pertinent to potential ultrafast laser operation.

2. Experimental

A $Li_2Gd_4(MoO_4)_7$ crystal doped with 3 mol.% Tm^{3+} ions concentration in the melt was grown by the Czochralski technique. Crystal pulling was performed in air using a platinum crucible. The detailed crystal growth procedure was described elsewhere [22]. Finally, a Tm^{3+}:$Li_2Gd_4(MoO_4)_7$ crystal with dimensions of Ø22 mm × 25 mm was obtained, as shown in Fig. 1.

The concentration of Tm^{3+} in the Tm^{3+}:$Li_2Gd_4(MoO_4)_7$ crystal was determined to be 1.90 at.% ($[Tm^{3+}] = 1.41 \times 10^{20}$ ions cm^{-3}) by inductively coupled plasma and atomic emission spectrometry (Ultima 2, Jobin–Yvon). Since $Li_2Gd_4(MoO_4)_7$ is an optically uniaxial crystal (tetragonal system) [21], a 1.0 mm thick plate sample cut from the crystal with the c-axis parallel to its main faces was used for the σ ($E \perp c$, $k \perp c$) and π ($E \parallel c$, $k \perp c$) polarized spectral measurements, where E, k, and c are the electric field, wave vector, and optical axis of the uniaxial crystal, respectively. The polarized absorption spectra were recorded by a UV–vis/NIR Spectrometer (Lambda900, PerkinElmer). The polarized fluorescence spectra from 600 nm to 1650 nm and fluorescence lifetimes of the $^1G_4$ and $^3H_4$ manifolds were measured using a Fluorescence Spectrophotometer (FLS920, Edinburgh). The polarized fluorescence spectra in the range of 1700–2050 nm and lifetimes of the $^3F_4$ manifold were investigated using another Spectrophotometer (FSP920C, Edinburgh). All the experiments were performed at room temperature.

3. Results and discussion

3.1. Absorption spectra and Judd–Ofelt analysis

The polarized absorption spectra of the Tm^{3+}:$Li_2Gd_4(MoO_4)_7$ crystal were measured in the 400–2000 nm spectral range at room temperature and presented in Figs. 2 and 3. All the absorption bands correspond to the transitions of Tm^{3+} from the ground state $^3H_6$ to the excited state J, which are marked in Fig. 2. The strong

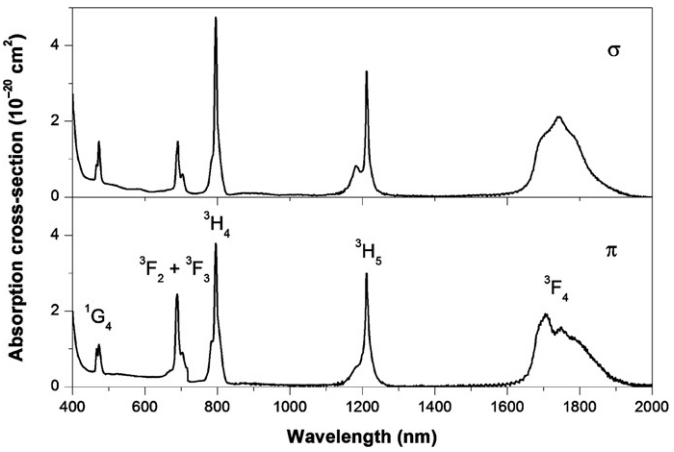

Fig. 2. Polarized absorption spectra of the Tm^{3+}:$Li_2Gd_4(MoO_4)_7$ crystal at room temperature.

absorption band around 800 nm is attributed to the $^3H_6 \rightarrow {}^3H_4$ transition (see Fig. 3), which coincides with the wavelength of radiation from a GaAlAs diode laser. For this transition, the full width at half the maximum (FWHMs) are 8.8 nm and 10.2 nm for the σ and π polarizations, respectively, which are typical for the majority of tetragonal DMo and DW crystals, e.g. Tm^{3+}:$NaGd(MoO_4)_2$ (7.0 nm and 35.0 nm for the σ and π polarizations) [24] and Tm^{3+}:$NaGd(WO_4)_2$ (8.0 nm for both σ and π polarizations) [25], but significantly greater than those of Tm^{3+}:YAG (4.0 nm) [23], Tm^{3+}:YVO_4 (5.0 nm for the π polarization) [9], and Tm^{3+}:$KY(WO_4)_2$ (5.4 nm for $E \parallel N_m$) [6]. Such broad bandwidths make the crystal very adequate for diode pumping, since wavelength requirements imposed on LDs are largely relaxed. The peak absorption cross-sections σ_{abs} are 4.69×10^{-20} cm^2 and 3.72×10^{-20} cm^2 at 795 nm for the σ and π polarizations, respectively. Thus, the crystal exhibits the largest value of σ_{abs} among the isostructural DMo and DW crystals except Tm^{3+}:$NaLa(MoO_4)_2$ (4.84×10^{-20} cm^2 for the σ polarization) [26] and Tm^{3+}:$NaGd(MoO_4)_2$ (5.2×10^{-20} cm^2 for the σ polarization) [27]. Additionally, regarding the tetragonal DT and DMo crystals, the peak σ_{abs} for the π polarization is generally much less than that for the σ polarization, e.g. σ_{abs} (π) = 1.59×10^{-20} cm^2, σ_{abs} (σ) = 4.33×10^{-20} cm^2 for Tm^{3+}:$LiGd(MoO_4)_2$ [17]. It is noteworthy that σ_{abs} (π) approaches σ_{abs} (σ) in the title crystal. Therefore, the Tm^{3+}:$Li_2Gd_4(MoO_4)_7$ crystal can be efficiently pumped by LD with both polarization configurations.

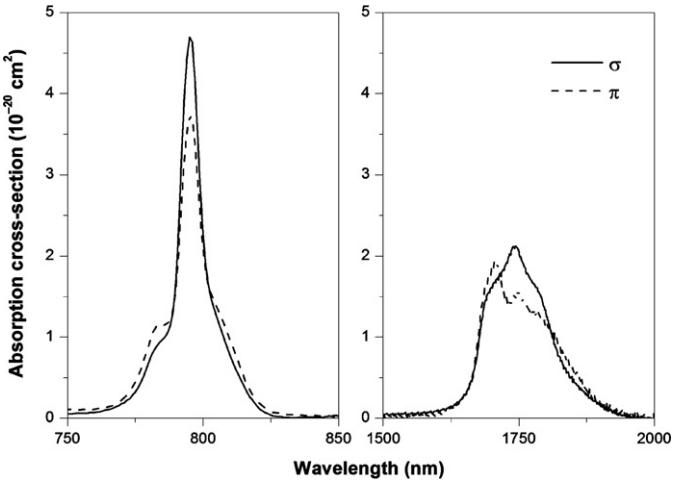

Fig. 3. Absorption cross-sections related to the $^3H_6 \rightarrow {}^3H_4$ and $^3H_6 \rightarrow {}^3F_4$ transitions.

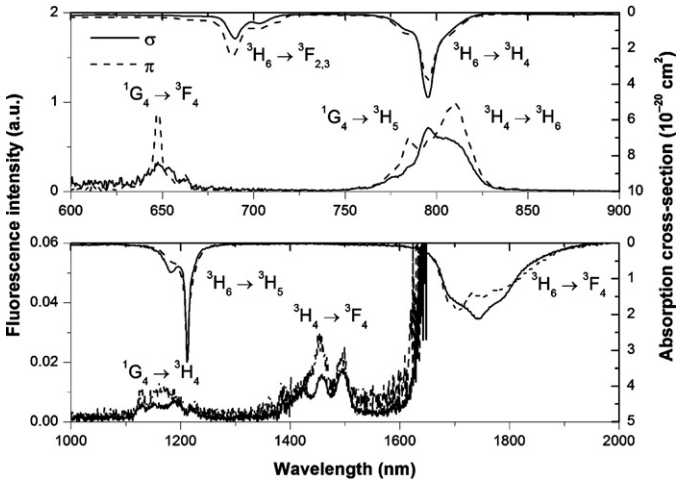

Fig. 4. Polarized fluorescence spectra of the Tm^{3+}:$Li_2Gd_4(MoO_4)_7$ crystal after $^1G_4$ excitation.

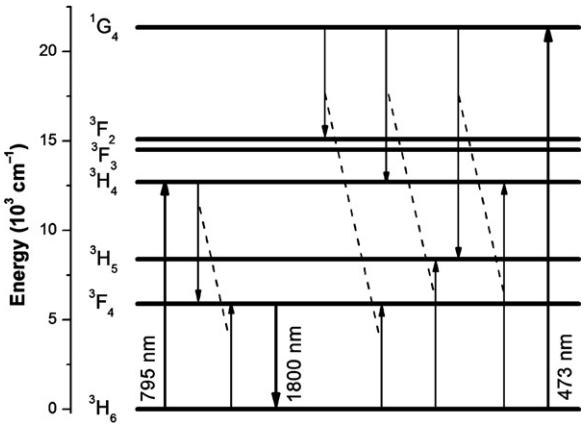

Fig. 5. The pumping and cross-relaxation mechanisms after $^3H_4$ and $^1G_4$ excitation.

The Judd–Ofelt theory has become a standard tool for evaluating the spectroscopic parameters of rare earth ions in crystals and glasses [28,29]. The calculation procedure follows that in Ref. [30]. The line strengths of the transitions are deduced from the analysis of the absorption spectra, and then the experimental data are fitted in accordance with the Judd–Ofelt parameterization scheme after subtraction of the magnetic dipole contribution for the $^3H_6 \rightarrow {}^3H_5$ transition. The magnetic dipole contribution is calculated in the light of the Refs. [31,32], and the reduced matrix elements are taken from Refs. [32,33]. The values of the refractive index n are derived from the Sellmeier equations established for the $Li_2Gd_4(MoO_4)_7$ crystal [1,34]:

$$n_o^2 = 1 + \frac{2.96911\lambda^2}{\lambda^2 - 0.02813} \quad (1)$$

$$n_e^2 = 1 + \frac{2.93595\lambda^2}{\lambda^2 - 0.02849} \quad (2)$$

The root-mean-square deviation between the experimental and calculated line strengths, RMS ΔS, is introduced to justify the fitting quality, which is expressed as:

$$\text{RMS } \Delta S = \sqrt{\frac{\sum_{i=1}^{N}(S_{\text{exp}} - S_{\text{cal}})^2}{N-3}} \quad (3)$$

where N is the number of transitions involved in the calculations.

The Judd–Ofelt parameters Ω_t (t = 2, 4, 6) can be subsequently used to assess the spontaneous emission probabilities, branching ratios and radiative lifetimes. The obtained spectroscopic data for the title crystal are summarized in Tables 1–3.

For the uniaxial crystal, the effective Judd–Ofelt parameters $\Omega_{t,\text{eff}}$ are defined as $\Omega_{t,\text{eff}} = (\Omega_{t,\pi} + 2\,\Omega_{t,\sigma})/3$. Table 2 provides the $\Omega_{t,\text{eff}}$ parameters of the crystals doped with Tm^{3+} and some other rare earth ions for comparison. It can be observed that all these crystals are characterized by a high Ω_2 parameter. Generally, the magnitude of Ω_2 depends on the local environment of the optically active ions [36]. A large value of Ω_2 reflects a high degree of covalency of the metal-ligand bond in the $Li_2Gd_4(MoO_4)_7$ matrix.

3.2. Fluorescence spectra and stimulated emission cross-sections

Fig. 4 depicts the polarized fluorescence spectra of the Tm^{3+}:$Li_2Gd_4(MoO_4)_7$ crystal after excitation into the $^1G_4$ manifold at 473 nm. The emission band at ~ 800 nm is due to the superposition of the $^1G_4 \rightarrow {}^3H_5$ and $^3H_4 \rightarrow {}^3H_6$ transitions [17,37], since these two transitions possess close barycentric wavelengths. The other three emission bands near 650 nm, 1150 nm, and 1450 nm can be assigned to the $^1G_4 \rightarrow {}^3F_4$, $^1G_4 \rightarrow {}^3H_4$, and $^3H_4 \rightarrow {}^3F_4$ transitions, respectively. As described in Fig. 4, the large overlap between the $^1G_4 \rightarrow {}^3H_5$ emission and the $^3H_6 \rightarrow {}^3H_4$ absorption indicates the possible existence of a resonant CR ($^1G_4 + {}^3H_6 \rightarrow {}^3H_5 + {}^3H_4$). Similarly, another possible resonant CR ($^1G_4 + {}^3H_6 \rightarrow {}^3H_4 + {}^3H_5$) is identified by the substantial overlap between the bands associated with the $^1G_4 \rightarrow {}^3H_4$ and $^3H_6 \rightarrow {}^3H_5$ transitions. Besides, a well-known phonon-assisted CR energy transfer process $^3H_4 + {}^3H_6 \rightarrow {}^3F_4 + {}^3F_4$, are also revealed in Fig. 4. The effectiveness of this process increases with the Tm^{3+} concentration and is usually high even for 1 at.% Tm^{3+}-doped systems [38]. It is worth emphasizing that this process which quenches the $^3H_4$ manifold and populates the $^3F_4$ manifold, facilitates the $^3F_4 \rightarrow {}^3H_6$ transition around 2 μm, since it transfers the excitation from the $^3H_4$ pump level to the $^3F_4$ upper laser level thus providing a so-called "two-for-one pumping" [39]. In summary, these CR channels sketched in Fig. 5, are supposed to remove the excitation of the $^1G_4$ and $^3H_4$ manifolds and hence lead to low quantum efficiencies, which will be discussed in Section 3.3.

Excitation into the $^3H_4$ manifold provides two fluorescence bands corresponding to the $^3H_4 \rightarrow {}^3F_4$ and the $^3F_4 \rightarrow {}^3H_6$ transitions within the measuring range, as demonstrated in Figs. 6 and 7.

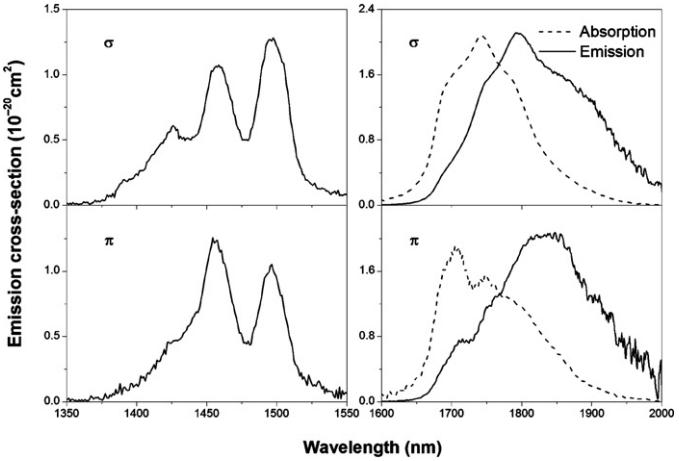

Fig. 6. Emission cross-sections associated with the $^3H_6 \rightarrow {}^3H_4$ and $^3F_4 \rightarrow {}^3H_6$ transitions for the Tm^{3+}:$Li_2Gd_4(MoO_4)_7$ crystal.

Table 1
Experimental and calculated line strengths of Tm^{3+} in the $Li_2Gd_4(MoO_4)_7$ crystal.

$^3H_6 \rightarrow$ J-manifold	π-polarization			σ-polarization		
	λ_a (nm)	S_{exp} (10^{-20} cm^2)	S_{cal} (10^{-20} cm^2)	λ_a (nm)	S_{exp} (10^{-20} cm^2)	S_{cal} (10^{-20} cm^2)
$^3F_4$	1749	10.37	10.37	1744	10.98	11.02
$^3H_5$	1212	3.45	3.78	1212	3.31	3.13
$^3H_4$	795	5.25	5.16	795	5.53	5.56
$^3F_{2,3}$	688	3.79	3.65	690	1.69	1.77
$^1G_4$	473	1.22	0.94	473	1.21	0.98
Ω_t (10^{-20} cm^2)	$\Omega_2 = 14.19$, $\Omega_4 = 2.97$, $\Omega_4 = 2.47$			$\Omega_2 = 19.46$, $\Omega_4 = 0.27$, $\Omega_6 = 1.53$		
RMS ΔS (10^{-20} cm^2)	0.33			0.22		

Table 2
The effective Judd–Ofelt parameters of the $Li_2Gd_4(MoO_4)_7$ crystals doped with Tm^{3+} and some other rare earth ions.

Crystals	Ω_2 (10^{-20} cm^2)	Ω_4 (10^{-20} cm^2)	Ω_6 (10^{-20} cm^2)	References
Nd^{3+}:$Li_2Gd_4(MoO_4)_7$	21.90	8.40	6.00	[35]
Dy^{3+}:$Li_2Gd_4(MoO_4)_7$	17.10	2.24	2.45	[1]
Er^{3+}:$Li_2Gd_4(MoO_4)_7$	14.30	2.81	1.32	[22]
Tm^{3+}:$Li_2Gd_4(MoO_4)_7$	17.70	1.17	1.84	This work

Table 3
Calculated spontaneous emission probabilities, branching ratios, and radiative lifetimes of Tm^{3+} in the $Li_2Gd_4(MoO_4)_7$ crystal.

Transitions	λ_{em} (nm)	π-polarization			σ-polarization			τ_{rad} (μs)
		A_{ed} (s^{-1})	A_{md} (s^{-1})	β	A_{ed} (s^{-1})	A_{md} (s^{-1})	β	
$^1G_4 \rightarrow {}^3H_6$	477	6090.7	0	0.519	6452.9	0	0.545	85.0
$^1G_4 \rightarrow {}^3F_4$	649	687.2	16.9	0.060	473.1	17.1	0.042	
$^1G_4 \rightarrow {}^3H_5$	781	3208.1	176.3	0.289	3076.5	178.5	0.275	
$^1G_4 \rightarrow {}^3H_4$	1170	1237.0	43.0	0.109	1432.5	43.6	0.125	
$^1G_4 \rightarrow {}^3F_3$	1485	207.2	4.6	0.018	130.2	4.7	0.011	
$^1G_4 \rightarrow {}^3F_2$	1633	55.1	0	0.005	26.5	0	0.002	
$^3H_4 \rightarrow {}^3H_6$	784	6117.0	0	0.901	6674.6	0	0.913	140.1
$^3H_4 \rightarrow {}^3F_4$	1432	551.4	28.7	0.085	574.7	29.1	0.083	
$^3H_4 \rightarrow {}^3H_5$	2166	79.4	12.0	0.014	22.0	12.1	0.004	
$^3H_5 \rightarrow {}^3H_6$	1224	1082.3	114.5	0.986	909.5	116.0	0.983	909.1
$^3H_5 \rightarrow {}^3F_4$	3826	16.6	0.3	0.014	17.5	0.3	0.017	
$^3F_4 \rightarrow {}^3H_6$	1799	1170.4	0	1.000	1264.7	0	1.000	810.9

In Fig. 6, the emission cross-sections near 1.5 μm are calculated according to the Füchtbauer–Ladenburg formula [40]:

$$\sigma_{em}(\lambda) = \frac{A\lambda^5 I(\lambda)}{8\pi c n^2 \int \lambda I(\lambda) d\lambda} \quad (4)$$

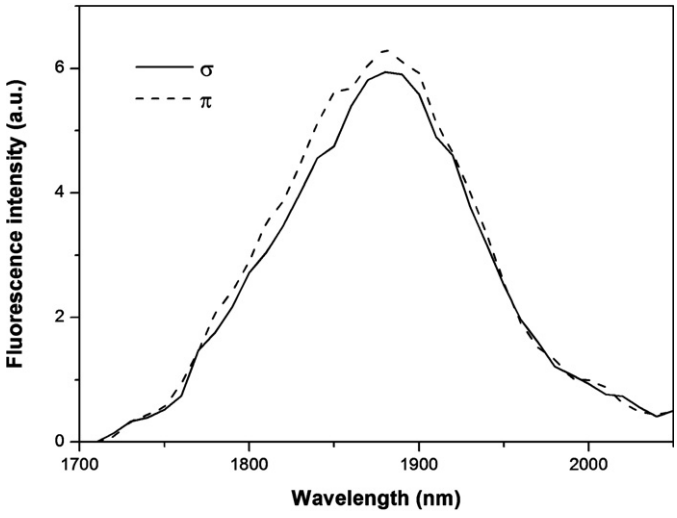

Fig. 7. Polarized fluorescence spectra near 2.0 μm after $^3H_4$ excitation.

The peak emission cross-sections σ_{em} are 1.28×10^{-20} cm^2 at 1497 nm for the σ polarization and 1.26×10^{-20} cm^2 at 1454 nm for the π polarization, respectively. The 1.5 μm emission via $^3H_4 \rightarrow {}^3F_4$ transition is of great interest, however, suffers from self-terminated laser operation because of τ_f ($^3H_4$) < τ_f ($^3F_4$). Consequently, it is a good choice to additionally dope with deactivators (e.g. Ho^{3+}, Tb^{3+}, or Eu^{3+}) so as to selectively depopulate the $^3F_4$ manifold [41].

Owing to the restriction of test instrument, we only obtained the uncalibrated fluorescence spectra around 2 μm, as shown in Fig. 7. These broad emission bands extend from 1710 nm to 2050 nm for both polarizations. The emission cross-section σ_{em}, providing important information about the potential laser performance of a material, can be calculated by the reciprocity method [42]:

$$\sigma_{em}(\lambda) = \sigma_{abs}(\lambda)\frac{Z_l}{Z_u}\exp\left(\frac{E_{zl} - h\lambda^{-1}}{k_B T}\right) \quad (5)$$

where Z_l and Z_u represent the partition functions of the lower and upper manifolds, and E_{zl} denotes the zero-line energy. Since the precise energy scheme of Tm^{3+} in the $Li_2Gd_4(MoO_4)_7$ crystal is not available yet, the values of E_{zl} and Z_l/Z_u are approximated by those obtained for Tm^{3+} in the isostructural $NaLa(MoO_4)_2$ crystal with similar crystal field intensity: $E_{zl} = 5595$ cm^{-1}, $Z_l/Z_u = 1.33$ [43]. Then, the calculated σ_{em} versus wavelength are plotted in Fig. 6. The maximum σ_{em} amount to 2.11×10^{-20} cm^2 at 1792 nm for the σ polarization and 2.08×10^{-20} cm^2 at 1847 nm for the π polarization. These values approach those of Tm^{3+}:$LiGd(MoO_4)_2$ (2.44×10^{-20} cm^2 at 1786 nm for the σ polarization and 2.07×10^{-20} cm^2 at 1838 nm for the π polarization)

Table 4
Spectral features of several promising Tm^{3+}-doped crystals.

	$Li_2Gd_4(MoO_4)_7$	$LiGd(MoO_4)_2$	$NaLa(MoO_4)_2$	$NaGd(WO_4)_2$	$KY(WO_4)_2$*
[Tm] (10^{20} cm^{-3})	1.41	3.56	4.40	2.34	2.20
λ_{abs} (nm)	795 (σ) 795 (π)	795 (σ) 781 (π)	795 (σ) 795 (π)	795 (σ) 795 (π)	801.6
$\Delta\lambda_{abs}$ (nm)	8.8 (σ) 10.2 (π)	8.0 (σ) 37.0 (π)	5.5(σ) 34.0 (π)	8.0 (σ) 8.0 (π)	5.4
$\sigma_{abs,max}$ (10^{-20} cm^2)	4.69 (σ) 3.72 (π)	4.33 (σ) 1.59 (π)	4.84 (σ) 1.57 (π)	2.90 (σ) 1.20 (π)	5.20
λ_{em} (nm)	1792 (σ)1847 (π)	1786 (σ)1838 (π)	1789 (σ)1837 (π)	1796 (σ)1847 (π)	1845 1910
$\Delta\lambda_{em}$ (nm)	188 (σ) 185 (π)	175 (σ) 160 (π)	145 (σ) 118 (π)	170 (σ) 170 (π)	100
$\sigma_{em,max}$ (10^{-20} cm^2)	2.11 (σ) 2.08 (π)	2.44 (σ) 2.07 (π)	1.91 (σ) 1.96 (π)	1.10 (σ) 1.00 (π)	4.20 1.15
τ_r ($^3F_4$) (ms)	0.91	0.93	1.10	1.35	1.11
References	This work	[17]	[24,27]	[25]	[6]

* Data for the E // N_m polarization in $KY(WO_4)_2$ is presented.

[17], and to our knowledge exceed those of other tetragonal DMo and DW previously reported [24–27].

As Tm^{3+} laser around 2 μm operates as a quasi-three-level system, the gain cross-section $\sigma_g(\lambda)$ are determined using the formula $\sigma_g(\lambda) = \beta\sigma_{em}(\lambda) - (1-\beta)\sigma_{abs}(\lambda)$, where β denotes the population inversion rate of Tm^{3+}. The result, presented in Fig. 8, implies both the achievable range of laser tuning in the absence of frequency selective elements in the laser cavity and the expected gain cross-sections at any wavelength within this range for a given β. The positive gains for $\beta = 0.4$ extend from 1795 nm to 2015 nm for the σ polarization and 1796 nm to 1995 nm for the π polarization, respectively.

3.3. Fluorescence lifetimes and quantum efficiencies

The fluorescence decay curves of the $^1G_4$, $^3H_4$ and $^3F_4$ manifolds of Tm^{3+} in the $Li_2Gd_4(MoO_4)_7$ crystal were recorded by monitoring the emissions of the $^1G_4 \rightarrow {}^3F_4$, $^3H_4 \rightarrow {}^3F_4$ and $^3F_4 \rightarrow {}^3H_6$ transitions at room temperature, as exhibited in Fig. 9. The lifetimes τ_f of the $^1G_4$, $^3H_4$ and $^3F_4$ manifolds are 37.2 μs, 90.0 μs and 1.8 ms, respectively.

The fluorescence quantum efficiencies, defined as $\eta = \tau_f/\tau_r$, are estimated to be 0.438 and 0.643 for the $^1G_4$ and $^3H_4$ manifolds. Such low values of η clearly reveal the contribution of nonradiative relaxation processes involving multiphonon and ion-ion interactions. The multiphonon relaxation for the $^3H_4$ manifold is inefficient owing to the wide energy gap between the $^3H_4$ level and the $^3H_5$ level (~4300 cm^{-1}) as compared with the maximum phonon energy of the $[MoO_4]^{2-}$ group (~880 cm^{-1} [44]). This has already been proved by the high η ($^3H_4$) observed in several dilute Tm^{3+}-doped molybdate crystals, such as $\eta = 0.854$ in 0.9 at.% Tm^{3+}:$LiGd(MoO_4)_7$ [17] and $\eta = 0.84$ in 0.59 at.% Tm^{3+}:$NaGd(MoO_4)_7$ [24]. Taking into account the larger energy gap between the $^1G_4$ and $^3F_2$ manifolds than that between the $^3H_4$ and $^3H_5$ manifolds, the multiphonon relaxation for the $^1G_4$ manifold should be much weaker than that for the $^3H_4$ manifold. Therefore, it can be concluded that the CR processes between Tm^{3+} levels (see Fig. 5) are the most probable reason for the low η of these two manifolds.

There is no CR scheme that may quench the $^3F_4$ manifold [45]. It is notable that τ_f ($^3F_4$) is remarkably longer than τ_r ($^3F_4$). Analogous behavior has also been observed in a number of Tm^{3+}-doped crystals [6,39]. The main reason for this discrepancy is that the reabsorption effect lengthens the measured lifetime significantly. To perform accurate measurement of the τ_f ($^3F_4$), the powder method is adopted in the present work, which is capable of efficiently suppressing this effect [46]. The bulk sample is ground to fine powder, and immersed into the monochlorobenzene ($n = 1.52$) which is used for refractive index matching. Detailed experimental processes can be found in Ref. [46]. The resultant τ_f ($^3F_4$) for the powder sample is 0.91 ms and much shorter than that for the bulk sample (1.80 ms). Furthermore, taking into account the intrinsic uncertainty of the Judd–Ofelt analysis (±20%), this value is close to that of τ_r ($^3F_4$).

Table 4 provides the spectral features of the Tm^{3+}:$Li_2Gd_4(MoO_4)_7$ crystal as compared with several promising Tm^{3+}-doped DMo and DT crystals. In contrast with the ordered monoclinic Tm^{3+}:$KY(WO_4)_2$ crystal in which pulse of 386 fs has been generated with an average power of 235 mW at 2029 nm [3], disordered tetragonal DMo and DMo crystals exhibit smaller peak cross-sections but larger optical bandwidths. It can follows from Table 4 that the Tm^{3+}:$Li_2Gd_4(MoO_4)_7$ crystal has similar spectral parameters to the tetragonal DMo crystals and slightly larger cross-sections than the isostructural DW crystals. Recently,

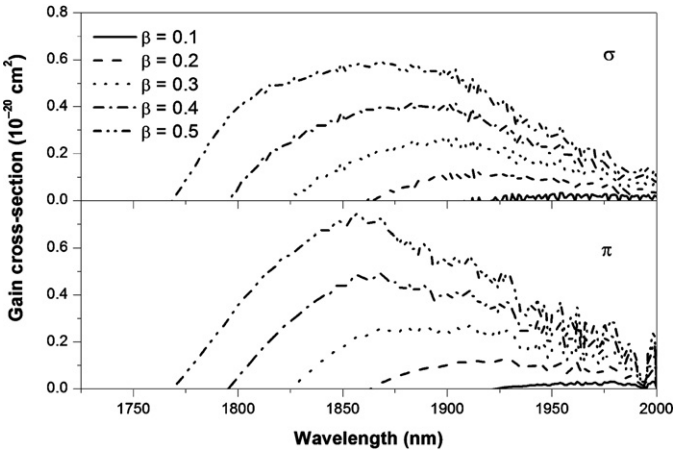

Fig. 8. Gain cross-sections of the $^3F_4 \rightarrow {}^3H_6$ transition for the Tm^{3+}:$Li_2Gd_4(MoO_4)_7$ crystal.

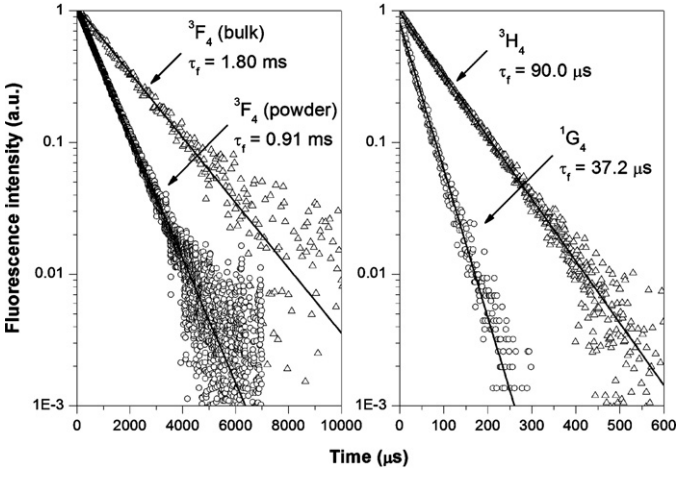

Fig. 9. Fluorescence decay curves of the $^3F_4$, $^3H_4$, and $^1G_4$ manifolds at room temperature.

the Tm^{3+}:$Li_{0.375}Lu_{0.375}Ba_{0.25}MoO_4$ crystal has demonstrated the best laser performance so far obtained from a Tm^{3+}-doped disordered crystal, and shown the potential of application in mode-locked sub-200 fs lasers [15]. It should be pointed out that the Tm^{3+}:$Li_2Gd_4(MoO_4)_7$ crystal possesses comparable optical properties with the Tm^{3+}:$Li_{0.375}Lu_{0.375}Ba_{0.25}MoO_4$ crystal. All these results suggest that the Tm^{3+}:$Li_2Gd_4(MoO_4)_7$ crystal is a promising gain medium for tunable and ultrafast (fs) pulse lasers.

4. Conclusions

A Tm^{3+}:$Li_2Gd_4(MoO_4)_7$ crystal has been successfully grown by the Czochralski method. Polarized absorption spectra, fluorescence spectra, and decay profiles have been recorded at room temperature. Compared with tetragonal DMo and DW crystals, the Tm^{3+}:$Li_2Gd_4(MoO_4)_7$ crystal possesses a similar scheelite-type disordered structure but different occupancy factors for M^+ and T^{3+}. As a consequence, the crystal exhibits similar spectral features to DMo and DW crystals, such as broad optical bandwidths, large absorption and emission cross-sections, and a long $^3F_4$ lifetime, which are good for the ultrafast laser action in the 2 μm spectral region. The main feature of the title crystal is the comparable values of σ_{abs} for the π and σ polarizations; hence, strong pump absorption and then efficient laser operation can be expected for both polarization configurations. To summarize, the Tm^{3+}:$Li_2Gd_4(MoO_4)_7$ crystal displays the potential for generation of subpicosecond (even sub-200 fs) laser pulses in the mode-locked regime.

Acknowledgment

This project was supported by the Nature Science Foundation of Education Department of Anhui Province (KJ2010B203, KJ2010B205), the Natural Science Foundation of Fujian Province (2011J01376), the National Natural Science Foundation of China (60808033, 61108054), and the Key Discipline Construction Project of Materials Science of Huainan Normal University.

References

[1] W. Zhao, W.W. Zhou, M.J. Song, G.F. Wang, J.M. Du, H.J. Yu, J.X. Chen, J. Alloys Compd. 509 (2011) 3937–3942.
[2] W. Zhao, Z.B. Lin, L.Z. Zhang, G.F. Wang, J. Alloys Compd. 509 (2011) 2815–2818.
[3] A.A. Lagatsky, S. Calvez, J.A. Gupta, V.E. Kuleshov, C.T.A. Brown, M.D. Dawson, W. Sibbett, Opt. Express 19 (2011) 9995–10000.
[4] P. Samuel, D. Thangaraju, S. Moorthy Babu, J. Alloys Compd. 509 (2011) 177–180.
[5] D. Kasprowicz, M.G. Brik, A. Majchrowski, E. Michalski, A. Biadasz, J. Alloys Compd. 509 (2011) 1430–1435.
[6] A.E. Troshin, V.E. Kisel, A.S. Yasukevich, N.V. Kuleshov, A.A. Pavlyuk, E.B. Dunina, A.A. Kornienko, Appl. Phys. B 86 (2007) 287–292.
[7] H. Li, L.Z. Zhang, Z.B. Lin, G.F. Wang, J. Alloys Compd. 493 (2010) 372–375.
[8] A.A. Lagatsky, X. Han, M.D. Serrano, C. Cascales, C. Zaldo, S. Calvez, M.D. Dawson, J.A. Gupta, C.T.A. Brown, W. Sibbett, Opt. Lett. 35 (2010) 3027–3029.
[9] K. Ohta, H. Saito, M. Obara, J. Appl. Phys. 73 (1993) 3149–3152.
[10] F. Haxsen, A. Ruehl, M. Engelbrecht, D. Wandt, U. Morgner, D. Kracht, Opt. Express 16 (2008) 20471–20476.
[11] W.B. Cho, A. Schmidt, J.H. Yim, S.Y. Choi, S. Lee, F. Rotermund, U. Griebner, G. Steinmeyer, V. Petrov, X. Mateos, M.C. Pujol, J.J. Carvajal, M. Aguiló, F. Díaz, Opt. Express 17 (2009) 11007–11012.
[12] J.F. Pinto, L. Esterowitz, G.H. Rosenblatt, Opt. Lett. 17 (1992) 731–732.
[13] M.J. Song, W. Zhao, G.F. Wang, M.L. Zhao, L.T. Wang, J. Alloys Compd. 509 (2011) 2164–2169.
[14] E.V. Zharikov, C. Zaldo, F. Díaz, MRS Bull. 34 (2009) 271–276.
[15] M. Rico, X.M. Han, C. Cascales, F. Esteban-Betegón, C. Zaldo, Opt. Express 19 (2011) 7640–7645.
[16] X.Y. Huang, W. Zhao, G.F. Wang, X.X. Li, Q.M. Yu, J. Alloys Compd. 509 (2011) 6578–6584.
[17] J.F. Tang, Y.J. Chen, Y.F. Lin, X.H. Gong, J.H. Huang, Z.D. Luo, Y.D. Huang, J. Opt. Soc. Am. B 27 (2010) 1769–1777.
[18] C.L. Sun, F.Y. Yang, T. Cao, Z.Y. You, Y. Wang, J.F. Li, Z.J. Zhu, C.Y. Tu, J. Alloys Compd. 509 (2011) 6987–6993.
[19] A. Schmidt, S. Rivier, V. Petrov, U. Griebner, X.M. Han, J.M. Cano-Torres, A. García-Cortés, M.D. Serrano, C. Cascales, C. Zaldo, J. Opt. Soc. Am. B 25 (2008) 1341–1349.
[20] R.K. Pandey, J. Phys. Soc. Jpn. 36 (1974) 177–178.
[21] L.H. Brixner, J. Phys. Soc. Jpn. 38 (1975) 1218.
[22] W. Zhao, L.Z. Zhang, G.F. Wang, J. Cryst. Growth 311 (2009) 2336–2340.
[23] T.Y. Fan, G. Huber, R.L. Byer, P. Mitzscherlich, IEEE J. Quantum Electron. 24 (1988) 924–933.
[24] W.J. Guo, Y.J. Chen, Y.F. Lin, X.H. Gong, Z.D. Luo, Y.D. Huang, J. Phys. D: Appl. Phys. 41 (2008) 115409.
[25] J.M. Cano-Torres, M.D. Serrano, C. Zaldo, M. Rico, X. Mateos, J.H. Liu, U. Griebner, V. Petrov, F.J. Valle, M. Galán, G. Viera, J. Opt. Soc. Am. B 23 (2006) 2494–2502.
[26] W.J. Guo, Y.J. Chen, Y.F. Lin, Z.D. Luo, X.H. Gong, Y.D. Huang, J. Appl. Phys. 103 (2008) 093106.
[27] Yu.K. Voron'ko, E.V. Zharikov, D.A. Lis, A.V. Popov, V.A. Smirnov, K.A. Subbotin, Phys. Solid State 50 (2008) 1605–1610.
[28] B.R. Judd, Phys. Rev. 127 (1962) 750–761.
[29] G.S. Ofelt, J. Chem. Phys. 37 (1962) 511–520.
[30] W. Zhao, W.W. Zhou, M.J. Song, G.F. Wang, J.M. Du, H.J. Yu, J.X. Chen, Optoelectron. Adv. Mater.-Rapid Commun. 5 (2011) 49–53.
[31] W.T. Carnall, P.R. Fields, K. Rajnak, J. Chem. Phys. 49 (1968) 4412–4423.
[32] N. Spector, R. Reisfeld, L. Boehm, Chem. Phys. Lett. 49 (1977) 49–53.
[33] W.T. Carnall, P.R. Fields, K. Rajnak, J. Chem. Phys. 49 (1968) 4424–4442.
[34] O.E. Bochkov, V.M. Gorbenko, Yu.V. Zabara, A.Yu. Kudzin, S.A. Flerova, Sov. Phys. Crystallogr. 22 (1977) 371–372.
[35] H.M. Zhu, Y.F. Lin, Y.J. Chen, X.H. Gong, Q.G. Tan, Z.D. Luo, Y.D. Huang, J. Appl. Phys. 102 (2007) 063104.
[36] F.A. Bol'shchikov, E.V. Zharikov, D.A. Lis, A.V. Popov, P.A. Ryabochkina, V.G. Senin, K.A. Subbotin, Opt. Spectrosc. 108 (2010) 743–752.
[37] L. Macalik, J. Hanuza, D. Jaque, J. García Solé, Opt. Mater. 28 (2006) 980–987.
[38] C. Li, A. Lagriffoul, R. Moncorge, J.C. Souriau, C. Borel, Ch. Wyon, J. Lumin. 62 (1994) 157–171.
[39] R. Lisiecki, P. Solarz, G. Dominiak-Dzik, W. Ryba-Romanowski, M. Sobczyk, P. Černý, J. Šulc, H. Jelínková, Y. Urata, Phys. Rev. B 74 (2006) 035103.
[40] B.F. Aull, H.P. Jenssen, IEEE J. Quantum Electron. 18 (1983) 925–930.
[41] W. Ryba-Romanowski, M. Berkowski, B. Viana, P. Aschehoug, Appl. Phys. B 64 (1997) 525–529.
[42] D.E. McCumber, Phys. Rev. 136 (1964) A954–A957.
[43] L.D. Merkle, J.B. Gruber, M.D. Seltzer, S.B. Stevens, T.H. Allik, J. Appl. Phys. 72 (1992) 4269–4274.
[44] T.T. Basiev, A.A. Sobol, Yu.K. Voronko, P.G. Zverev, Opt. Mater. 15 (2000) 205–216.
[45] W. Ryba-Romanowski, S. Gołvab, I. Sokólska, G. Dominiak-Dzik, J. Zawadzka, M. Berkowski, J. Fink-Finowicki, M. Baba, Appl. Phys. B 68 (1999) 199–205.
[46] M.C. Pujol, M.A. Bursukova, F. Güell, X. Mateos, R. Solé, J. Gavaldà, M. Aguiló, J. Massons, F. Díaz, P. Klopp, U. Griebner, V. Petrov, Phys. Rev. B 65 (2002) 165121.